An Evaluation of a 1/18° Resolution Regional Ocean Circulation Model of CROCO in the Southern Sunda Shelf

Apriansyah[1,3]*, Agus S. Atmadipoera[2], Indra Jaya[2], Dwiyoga Nugroho[4], Mohd. Fadzil Akhir[5]

[1]*Graduate School in Marine Sciences, IPB University*
Jl. Rasamala, Kampus IPB Darmaga Bogor 16680, West Java, Indonesia
[2]*Department of Marine Science and technology, IPB University*
Jl. Rasamala, Kampus IPB Darmaga Bogor 16680, West Java, Indonesia
[3]*Marine Science Department, Faculty of Mathematic and Natural Sciences, Tanjungpura University*
Jl. Prof.Dr.H.Hadari Nawawi Pontianak , Kalimantan Barat 78124, Indonesia
[4]*Oceanographic Research Center, National research and Innovation Agency*
Jl. Pasir Putih Raya No.1, RT.8/RW.10, Ancol, Daerah Khusus Ibukota Jakarta 14430
[5]*Institute of Oceanography and Environment, Universiti Malaysia Terengganu*
21030, Kuala Nerus, Terengganu, Malaysia
Email: apriansyah@fmipa.untan.ac.id

Abstract

The Coastal and Regional Ocean Community Model (CROCO) was applied to simulate the three dimensional ocean circulation on the southern Sunda Shelf with a horizontal resolution of 1/18° and 40 vertical layers. This configuration is called as CROCO18-SSS. The initial and open boundary conditions were derived from a global reanalysis product at a resolution of 1/12° from the Copernicus Marine Environment Monitoring Service (CMEMS). The regional model was driven by atmospheric, tides, and river discharges data from a wide variety of datasets, each with a different resolution. To test the model performance and capabilities of the CROCO18-SSS model outputs including sea level anomaly, current velocity, temperature, salinity, and volume transport, we have compared in the simulation results with other reanalysis product and satellite-derived datasets. The CROCO18-SSS model outputs reproduced the regional ocean circulation well from observations and reanalysis products. For example, the reversal of the monsoonal current in the southern sunda shelf, as well as strong persistent southward Makassar throughflow and their interaction in the southern Makassar Strait, can be seen clearly. The vertical structure of the zonal current component was comparable to that of the reanalysis product reference. The seasonal shift in temperature and salinity, with the water becoming colder and saltier during the northwest monsoon and warmer and fresher during the southeast monsoon, was also accurately reproduced by the CROCO18-SSS model. Additionally, the mean volume transport calculated by the CROCO18-SSS model for the Makassar and Karimata Straits was comparable to that reported in previous studies.

Keywords: *evaluation, satellite, reanalysis, southern sunda shelf, CROCO modelling system*

Introduction

Ocean modelling has long been used to study ocean dynamics and water mass stratification (Tranchant *et al.*, 2016); and to analyze oceanographic phenomena, such as fronts (Ismail and Ribbe, 2019), upwelling (Kok *et al.*, 2017), eddies (Horhoruw *et al.*, 2020), barotropic and baroclinic tides (Koropitan and Ikeda, 2008; Nugroho *et al.*, 2018; Katavouta *et al.*, 2022), and ocean current systems (Tozuka *et al.*, 2009; Susanto *et al.*, 2012; Wei *et al.*, 2016). Some benefits of using ocean modelling are as tools to better understand and to evaluate the physical processes and dynamics of ocean phenomena, which could contribute to the enhancement of our knowledge in the field of marine science and technology.

The Coastal and Regional Ocean Community model (CROCO) has been developed to investigate the ocean circulation dynamics. It is a recent hydrodynamic modelling system based on ROMS-AGRIF (Shchepetkin and McWilliams, 2005; Debreu *et al.*, 2012). It adopts surface- and terrain-following curvilinear coordinates (Shchepetkin and McWilliams, 2005). The model is capable to address coastal phenomena and their interactions with the open sea. Previous studies have applied CROCO modelling to study atmospheric wave-ocean coupling (Uchiyama *et al.*, 2010), internal waves, sediments (Blaas *et al.*, 2007), and biogeochemistry (Gutknecht *et al.*, 2013). It has also been applied to study the coastal front (Ismail and Ribbe, 2019), impact of rivers on ocean circulation (Ramadhan *et al.*, 2021), oil spill prediction (Nugroho *et al.*, 2021), and

*) Corresponding author

https://ejournal.undip.ac.id/index.php/ijms
DOI: 10.14710/ik.ijms.28.1.12-26
Received : 06-10-2022
Accepted : 10-01-2023

structure of coastal upwelling dynamics (de Mello *et al.*, 2022).

The bathymetry in the southern Sunda shelf is less than 70 m-depth which is dominant in the model domain, including the Karimata Strait, Java Sea, the western Flores Sea, and the southern part of Makassar Strait (Sarr *et al.* 2019). The seasonal reversal of the Asian-Australian monsoon system (NWM – northwest monsoon and SEM – southeast monsoon) strongly influences the SSS ocean dynamics (Wyrtki, 1961; Hamzah *et al.*, 2020). During the NWM period (December to February), northwesterly winds are fully developed, which is associated with the rainy season. In contrast, during the SEM period (June to August), southeasterly monsoon winds blow with dry air masses from the Australian Continent. Consequently, surface current distribution and oceanographic parameters are strongly controlled by the monsoon system (Apriansyah *et al.*, 2022). The ocean dynamics of SSS waters are also influenced by the Sunda Shelf Throughflow (Apriansyah and Atmadipoera, 2020), Indonesian Throughflow (ITF) from the Makassar Strait (Gordon, 2005; Du and Qu, 2010), complex bathymetry, unique atmospheric characteristics (Yulihastin *et al.*, 2021), tides (Nugroho *et al.*, 2018; Katavouta *et al.*, 2022), and rivers (Ramadhan *et al.*, 2021). The complex bathymetry, atmosphere, ocean dynamics, tides, and river runoff surrounding SSS must be considered as model inputs.

In this study, we have performed a higher resolution CROCO modelling that was applied to simulate ocean circulation in the southern Sunda Shelf (SSS). This study focused on evaluating the model capability and confidence for some model output variables, such as current velocity, sea level anomaly, temperature, salinity, and volume transport, by comparing the model output dataset with the reanalysis products and satellite-derived datasets. Other related papers from this simulation may be discussed elsewhere. Therefore, this study evaluates the performance of the model output from a realistic 3-dimension hydrodynamic model of CROCO and to investigate seasonal variations in ocean circulation and its variability in the Sunda Shelf waters.

Materials and Methods

The regional model configuration of the southern Sunda Shelf water was determined using CROCO version 1.2. The model domain was set up with a spatial resolution of 1/18° (approximately 5 km) and 40 vertical layers, with much denser vertical layers near the surface. This configuration is referred to as CROCO18-SSS.

This study used vertical S-coordinate stretching parameters of $\theta_s = 7$, $\theta_b = 1$, and $h_c = 2m$, which increased vertical resolution at the surface. A minimum depth of 5 m was selected for the study. The specified value cannot be zero, and must be set based on the horizontal resolution of the model grid. The bathymetric model was derived using the topography of the General Bathymetric Chart of the Oceans (GEBCO) gridded dataset for 15 s (Weatherall *et al.*, 2015). The slope parameter was 0.25, which prevented horizontal pressure gradient errors (Ismail and Ribbe, 2019). The bottom friction coefficient was

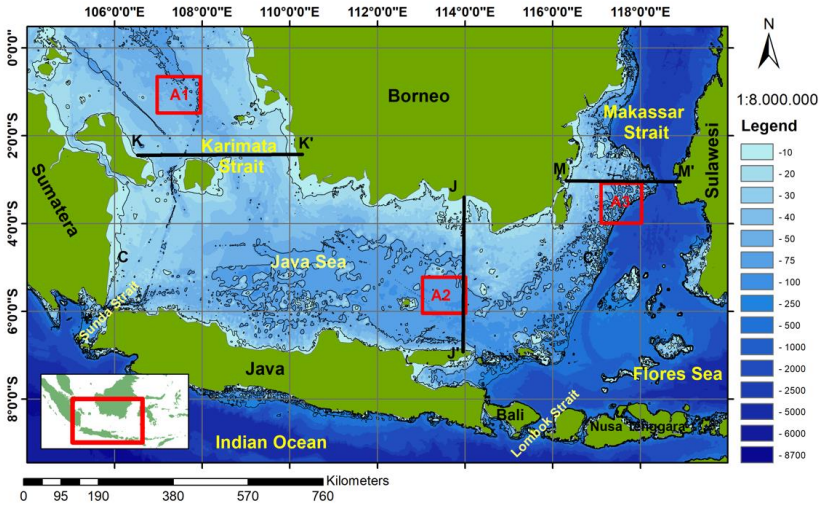

Figure 1. The bathymetry of the southern Sunda Shelf region was derived from GEBCO with contour intervals of 50, 100, and 200 m. The red boxes (A1, A2, and A3) denote the SLA time-series calculations for the CROCO18-SSS and other datasets. Black lines (KK') and (MM') are transects for volume transport calculation in Karimata Strait Transport (KST) and Makassar Strait Transport (MST). The black line (JJ') represents the vertical distribution of the zonal current component, temperature, and salinity.

calculated using logarithmic law (bottom roughness = 0.01) (Malauene *et al.*, 2018). Ganju and Sherwood, (2010) provided further details regarding the algorithm that parameterizes bottom roughness in an ocean model.

The momentum term uses 3rd-order upstream biased advection and 4th-order centered advection with harmonic averaging for vertical advection. For vertical mixing, K-profile (KPP) parameterization was used, and for lateral tracer advection, a split and rotated 3rd-order upstream biased lateral tracer scheme was used. Flather open boundary conditions for barotropic velocities and radiative open boundary conditions (Nugroho *et al.*, 2021).

The hydrodynamic model configuration was applied using the ROMS_TOOLS toolbox (Penven *et al.*, 2008). The model area stretches from 104 °E to 120 °E and 9.5 °S to 0.5 °N (Figure 1.). The open boundaries were set up on the northern, eastern, southern, and western sides of the model domain. The lateral boundary conditions were obtained from the GLORYS12V1 reanalysis product (Lellouche *et al.*, 2018), with a horizontal resolution of 1/12^o and a time span from 2010 to 2020. Table 1 presents the setup of the CROCO18-SSS configuration.

The model is forced by atmospheric parameters and river discharge along its open lateral boundaries by tides and oceanic conditions. Atmospheric forcings were obtained from ERA5 data (Hersbach *et al.*, 2020). ERA5 is the fifth generation of the ECMWF's atmospheric reanalysis of global climate (European Center for Medium-Range Weather Forecast, ECMWF). Surface forcing encompasses precipitation, air pressure, relative humidity, air temperature, shortwave and longwave radiation, and wind stress imposed from the ERA5 reanalysis at a 1/4^o horizontal resolution. Explicit tidal forcing was obtained from the TPXO.9v4 dataset at a resolution of 1/6^o horizontally (Egbert and Erofeeva, 2002). The 10 tidal constituents (K1, O1, Q1, P1, M2, N2, S2, K2, Mm, and Mf) were used as the open boundaries. The daily river discharge from the Global Flood Awareness System (GloFas) at a resolution of 1/10^o (Harrigan *et al.*, 2020) was applied at the river mouths along the coastlines of the study area. River discharge-point sources were mostly available along the coastlines of the model domain. There were 117 river sources, with an average discharge of above 50 $m^3.s^{-1}$. GloFas was chosen because it has been validated by field measurements in a study by Ramadhan *et al.* (2021). The CROCO18-SSS simulations ran from January 1, 2009, to December 31, 2020, with a 1-year spin-up (2009).

Data comparison

The model outputs of CROCO18-SSS were compared with the observational satellite-derived dataset and reanalysis product dataset to test the model performance and confidence. The observational satellite-derived dataset consisted of sea level anomalies (SLA), temperature, and salinity. Daily SLA data were obtained from the DUACS satellite, with a horizontal resolution of 1/4^o (Taburet *et al.*, 2019). Sea surface temperature data were obtained from the OSTIA satellite system, with a horizontal resolution of 1/20^o (Good *et al.*, 2020). Salinity data were obtained using a multivariate optimal interpolation algorithm that combined SMOS satellite images, in situ salinity measurements, and satellite SST information. The products were developed by COnsiglio Nazionale delle Ricerche (CNR) (Droghei *et al.*, 2016). The data were collected weekly at a horizontal resolution of 1/4^o on January 1, 1993. Multisensory satellite observational datasets were obtained from http://marine.copernicus.eu. Additional datasets from the GLORIS12V1 reanalysis products (SLA, current, salinity, and temperature) were also used for comparison, obtained from https://marine.copernicus.eu, based on the reanalysis products of the model and assimilation of

Table 1. Model configuration of CROCO18-SSS

Parameter	Value	Description
LLm0	286	Dimension in the ξ-direction
MMm0	180	Dimension in the η-direction
N	40	Number of vertical levels
dt	120	Model time step
NFAST	90	Number of barotropic time steps within one baroclinic time step
θ_s	7	Vertical S-coordinate surface stretching parameter
θ_b	1	Vertical S-coordinate bottom stretching parameter
h_c	2	Vertical S-coordinate *hc* parameter

observations with a resolution of 1/12°. The GLORYS12V1 reanalysis product dataset was validated using an observational dataset (Drévillon *et al.*, 2021).

Data analysis

To evaluate the CROCO18-SSS simulation, several model output variables (temperature, salinity, SLA, currents, and volume transport) were analyzed. The CROCO18-SSS output parameters were compared with GLORYS12V1 reanalysis and satellite-derived data. Seasonal and spatial variation of dataset (zonal and meridional currents, temperature, and salinity) were analyzed and contrasted between different monsoon periods (the NWM and SEM).

Climatology analysis or the annual cycle of parameters to investigate the seasonal cycles of the parameters (temperature and salinity) is calculated using Eq.1 below. The climatology method follows Thomson and Emery (2014):

$$\bar{X}(x,y) = \frac{1}{n}\sum_{i=1}^{n} x_i\left(x,y,t\right) \quad (1)$$

where: $\bar{X}(x,y)$ is the monthly average value at the position (x,y); $x_i(x,y,t)$ is the *i*-th value of data at position (x,y) and time *t*; n is data (i.e., from 2010 to 2020)

Estimates of transport volume in the Karimata Strait (KST) along the latitude section of 2.75 °S (KK' in Figure 1.), and in the Makassar Strait (MKT), along the latitude of 3°S (MM' in Figure 10.) were calculated using Eq. 2 below, following Fang *et al.*, (2010):

$$VT = \int_A v dA \quad (2)$$

where: v denotes meridional velocity (m/s), dA shows the area elements of the PP' and QQ' transects. The VT value was expressed in units of Sv (1 Sv = 10^6 $m^3.s^{-1}$).

Taylor diagram analysis (Taylor, 2001) was used to evaluate the correlation coefficient, standard deviation, and root mean squared deviation between the CROCO18-SSS dataset, GLORYS12V1 reanalysis dataset, and satellite data such as sea level anomalies, temperature, salinity, and volume transport. The scale value of Taylor diagram ranges between 0 and 1. Model performance improves if the correlation coefficient is close to 1. The RMSD and standard deviation near 0 indicated high accuracy.

Result and Discussion

Surface current

The CROCO18-SSS surface current simulation matched the GROLYS12V1 reanalysis product (Figure 2). Surface currents in the SSS are caused by wind stress, which varies seasonally (Kok *et al.*, 2021).

During the NWM (December–February), northwest monsoon winds pushed the Karimata Strait surface currents to the south. This current then turned eastward and was joined by a monsoon-generated surface current in the Java Sea. The eastward surface current splits in the eastern Java Sea, whereas one part continues to the Flores Sea and the remaining current turns northward and joins the southward Makassar throughflow current (Figure 2a, b.). During the SEM (June–August), the southeast monsoon winds drove the surface currents westward (Figure. 2b, d.). In the southern Makassar Strait, the southward-flowing current divides; one part exits directly into the Indian Ocean through the Lombok Strait, and the rest turns westward and joins the Java Sea surface current. Lombok is one of the three main exit passages of the ITF, besides the Ombai Strait and Timor passages (Atmadipoera *et al.*, 2009). The westward surface current from the Flores Sea extends towards the Java Sea during this period. Owing to the southeast monsoon, this current turns north in the Karimata Strait and joins farther the western boundary current along the Malaysia coast.

Figure 3 compares the vertical distribution of the current zonal component passing through the JJ' transect at 114° E. During the NWM, the zonal current was dominated by eastward flow towards the Flores Sea – Makassar Strait with a maximum speed of 0.4 $m.s^{-1}$near the northern coast of Java (7°S). This current originates from the water from the South China Sea, which enters the Java Sea via the Karimata Strait. The current appeared to weaken as the depth increased. In the SEM period, the zonal current flow was dominated by westward flow with a maximum velocity (~0.1 $m.s^{-1}$). This flow originated from the Makassar Strait Sea during this season.

Monsoon winds generated most of the water entering the Java Sea during the NWM and SEM periods (Fang *et al.*, 2010). In the NWM season, there is a north-south sea level slope between the Natuna Sea and the Java Sea (Fang *et al.*, 2010). This pressure gradient created a horizontal pressure gradient that drove the Sunda Shelf Throughflow (SSTF). The SSTF carries water masses from the South China Sea to Java Sea. During the SEM season, the mass of water in the Java Sea area also comes from ITF-Makassar.

There was a reasonable difference in the current patterns between the CROCO18-SSS and GLORYS12V1 reanalysis models during NWM and SEM. As shown in CROCO18-SSS, there was an eastward flow at 7° S during SEM. The eastward flow was observed between 4°S and 6°S in the GLORYS12V1 results. This difference may be related to the differences in the configuration of the model data, bathymetry, model parameter settings, and forcing data. The current pattern across the Java Sea was consistent between the CROCO18-SSS and GLORYS12V1 results during both NWM and SEM periods.

Sea Level Anomaly (SLA)

Figure 4 compares between the daily sea level anomalies (SLA) of the CROCO18-SSS, GLORYS12V1 reanalysis, and satellite data. It was revealed that the fluctuation of the daily SLA model was mostly similar to the observed data, showing a similar trend and amplitude at all three stations (Figure 4a, c, e.). The CROCO18-SSS – GLORYS12V1 and CROCO18-SSS -

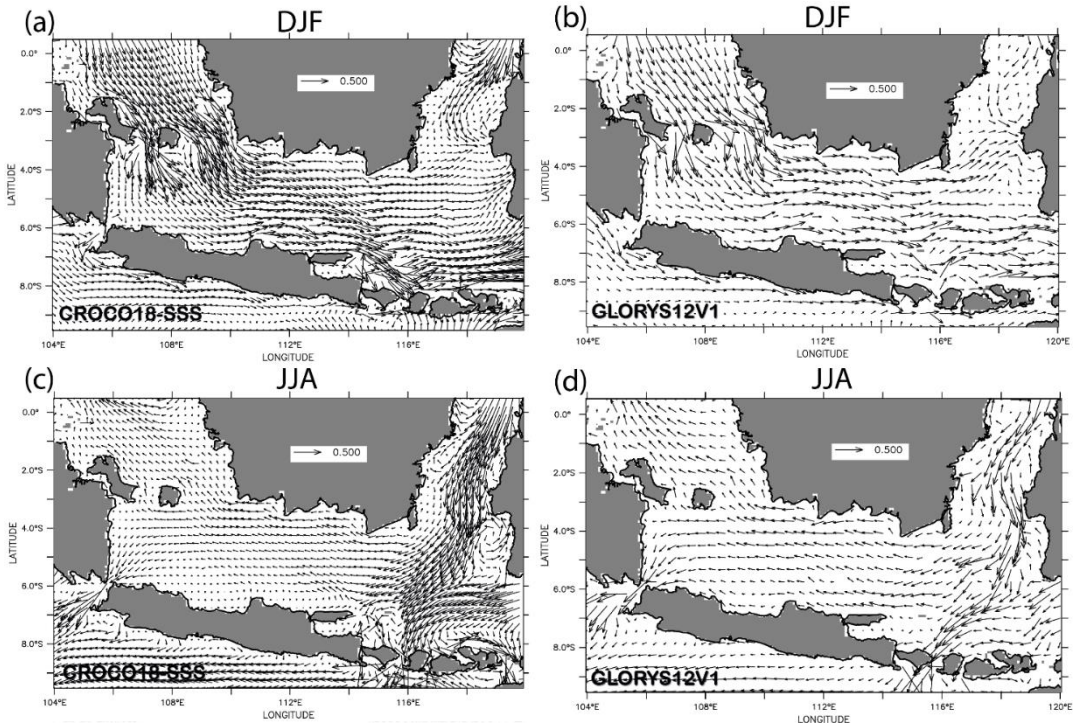

Figure 2. Seasonal surface current (m/s) during the Northwest monsoon (a, b) and (Southeast Monsoon (c, d) derived from CROCO18-SSS (left panel) and GLORYS12V1 (right panel)

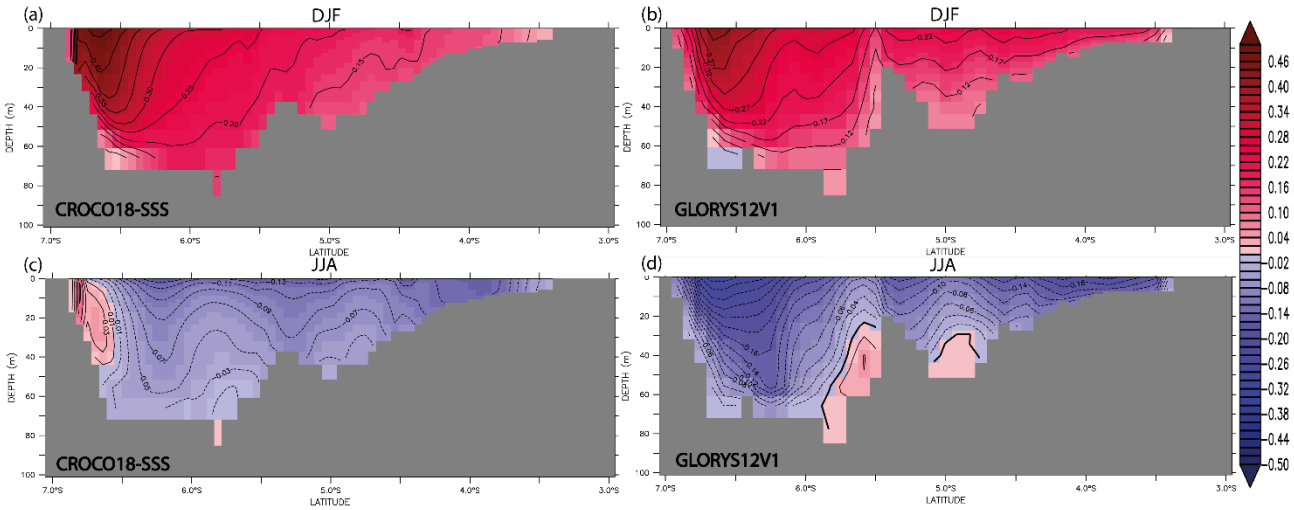

Figure 3. Seasonal vertical distribution of zonal current component (m/s) during the Northwest monsoon (a, b) and Southeast Monsoon (c, d) derived from CROCO18-SSS (left panel) and GLORYS12V1 (right panel). A positive (negative) value suggests easterly (westerly) movement through the Java Sea. (Line JJ' in Figure 1)

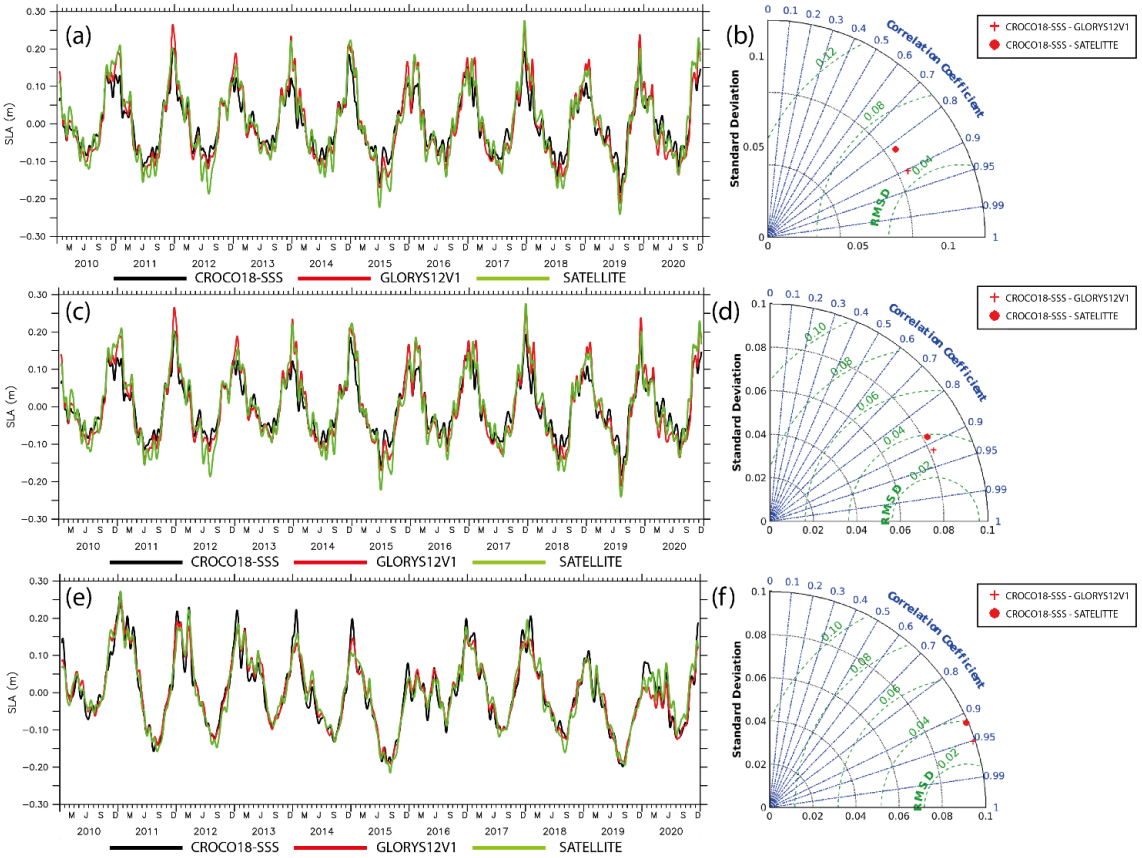

Figure 4. Daily sea levels anomaly (a, c, e, (m)) and Taylor diagram (b, d, f) derived from CROCO18-SSS (black lines), GLORYS12V1 (red lines), and satellite (green) at Karimata strait (upper), Java Sea (middle), and Makassar Strait (lower) (referred in Figure 1 (A1, A2, A3))

satellite comparisons in the Taylor diagram (4b, d, f) display correlation coefficients above 0.8 for all stations (A1, A2, A3). The root means square deviation (RMSD) of the daily SLA between the CROCO18-SSS model and the comparison data (GLORYS12V1 and satellite) was less than 0.05 for all stations (A1, A2, A3). Overall, CROCO18-SSS simulated the SLA in good agreement with satellite observations and GLORIS12V1 reanalysis.

In addition, the daily SLA for all stations exhibited large seasonal fluctuations in SLA, associated with the seasonal reversal of monsoon winds over the region. This is in accordance with previous studies (Kok *et al.*, 2021).

Sea surface temperature and salinity

Monsoonal winds are the main forcing that controls physical processes and dynamics over the Sunda Shelf region, causing large seasonal changes in sea surface temperature and salinity as well as seasonal reversal currents in this region. Figure 5 shows the validation results among the CROCO18-SSS data, GLORYS12V1 reanalysis, and the satellite-derived dataset of sea surface temperature and salinity at the A2 sampling location (referred to in Figure 1.). The correlation coefficient for temperature was above 0.90. The RMSD estimates are below 0.38 °C. The correlation coefficient for salinity was 0.95, and the comparison between the model salinity CROCO18-SSS and satellite-derived data was 0.76. The RMSD between model-reanalysis dataset and model-satellite dataset are 0.28 psu and 0.50 psu, respectively. The Taylor diagram for sea surface temperature and salinity (Figure 5.) revealed that the CROCO18-SSS model reproduced the available reanalysis and satellite-derived datasets well.

During the NWM, colder (Figure 6a–c.) and saltier (Figure 7a–c.) water masses flowed southward and joined warmer, fresher water masses in the Java Sea. High precipitation rates during this rainy season significantly contribute to large seasonal salinity variations in the Java Sea (Nuryanto *et al.*, 2016; Yulihastin *et al.*, 2021). Many big rivers discharged into the Java Sea also reduce the salinity (Ramadhan *et al.*, 2021).). In the Java Sea, eastward monsoonal currents bring cooler and fresher water masses into the southern Makassar Strait. According to Tozuka *et al.* (2009), the arrival of this fresher water mass

creates a north-south horizontal pressure gradient associated with northward surface flow in the upper 50 m and reducing Makassar throughflow in the thermocline layer. This pressure gradient creates a salinity gradient in the southern Makassar Strait.

During the SEM period, colder (Figure 6d–f.) and saltier (Figure 7d–f.) water masses were dominant in the eastern Java Sea and south of Makassar Strait. Water masses from Makassar throughflow as well as from upwelling water in the southern Makassar Strait contribute to variations in temperature and salinity in the region (Atmadipoera and Widyastuti, 2015; Utama *et al.*, 2017). Figures 2, 6, and 7 show that westward surface currents also bring colder and saltier water masses from the Flores Sea to Java Sea. In the Java Sea, less salty water mass derived from large river discharges is still present and mixed with saltier water mass from the Flores Sea, causing much lower saline water mass. Westward monsoonal current transports colder and fresher Java Sea water as far as crossing equator line near the Karimata Strait.

Figure 8 shows the vertical distribution of water temperature in the Java Sea during the NWM (a, b) and SEM (c, d) periods. During the NWM period, there was no stratification of the temperature distribution from the surface to the bottom. Stratification occurred at the bottom of the water during the SEM season. During the NWM period, the water mass of the SCS entered the Karimata Strait, influencing the temperature of the Java Sea. Despite more frequent precipitation during the NWM period, the water temperature was relatively lower than that during the SEM period. This was caused by colder water masses from the Makassar Strait and Flores Sea entering Java Sea during the SEM period. This cold temperature is primarily caused by upwelling in the southern Makassar Strait (Atmadipoera and Widyastuti, 2015; Utama *et al.*, 2017; Purba and Khan, 2019).

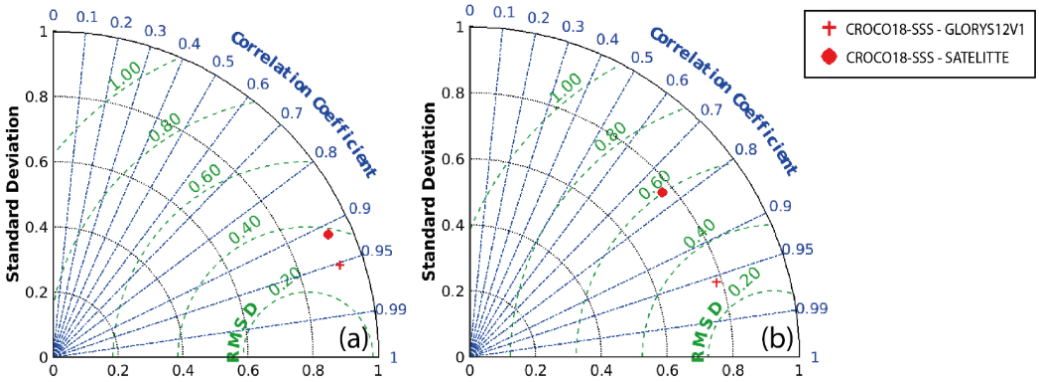

Figure 5. Taylor diagram for sea surface temperature (a) and salinity (b) derived from CROCO18-SSS, GLORYS12V1 and satellite in the Java Sea (referred sampling box A2 in Figure 1.).

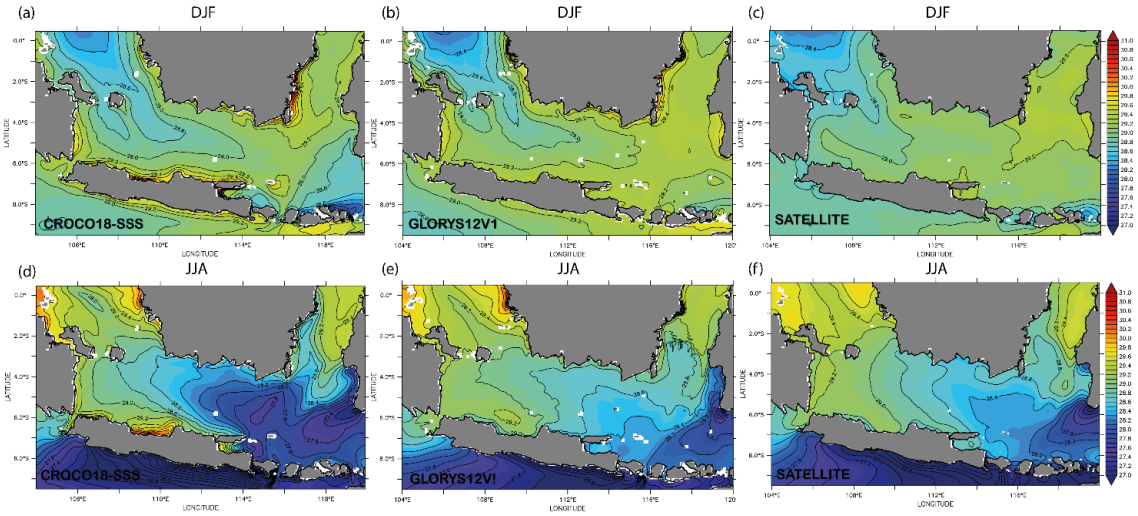

Figure 6. Seasonal sea surface temperature (°C) climatology during the (a–c) NWM and (d-f) SEM periods derived from CROCO18-SSS (left panel), GLORYS12V1 (middle panel) and satellite-derived data (right panel).

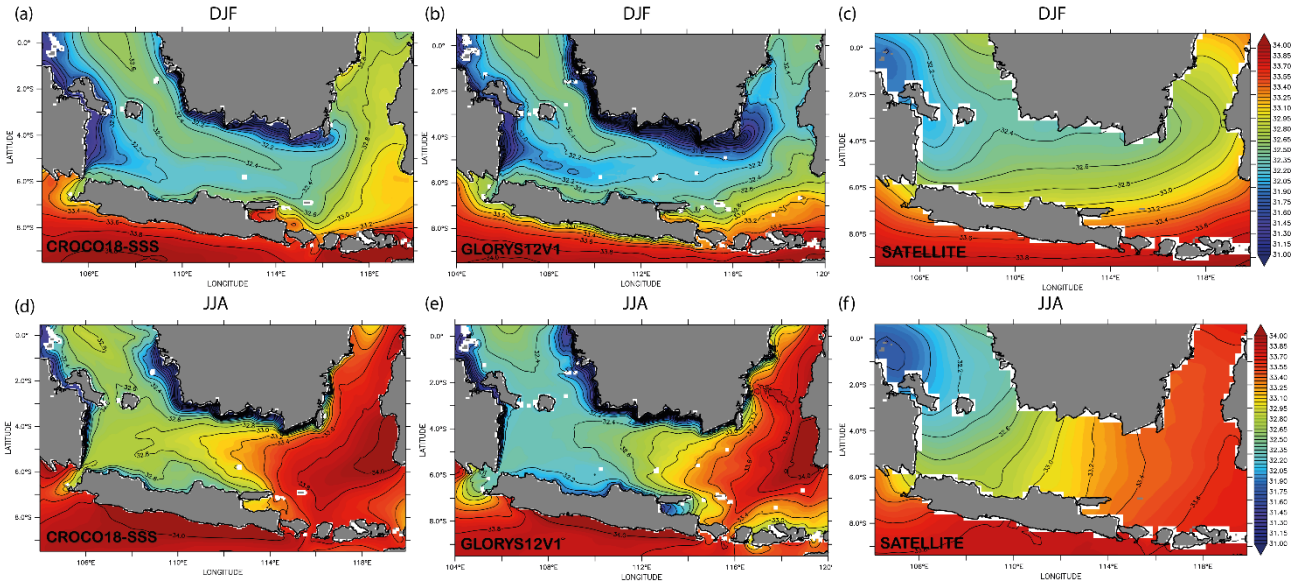

Figure 7. Seasonal sea surface salinity (psu) climatology during the (a–c) NWM and (d-f) SEM derived from CROCO18-SSS (left panel), GLORYS12V1 (middle panel) and satellite (right panel).

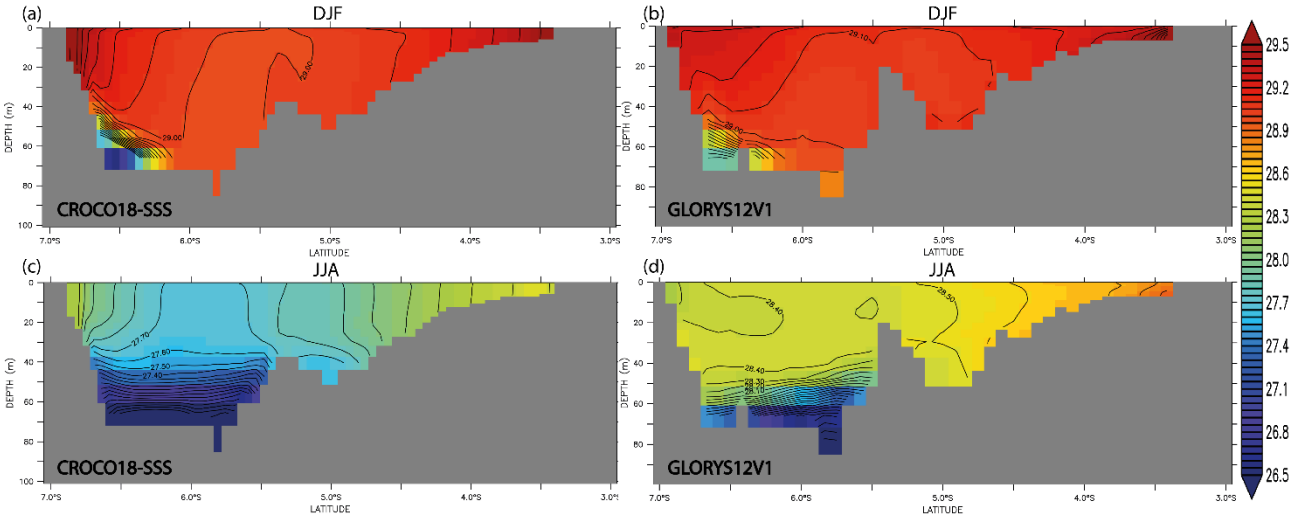

Figure 8. Seasonal vertical distribution of temperature (°C) during the Northwest monsoon (a, b) and (Southeast Monsoon (c, d) derived from CROCO18-SSS (left panel) and GLORYS12V1 (right panel). (Line JJ' in Figure 1.).

Figure 9 depicts the vertical salinity distribution in Java Sea waters along the 114°S transect during the NWM (a, b) and SEM (c, d) periods. During the NWM period, there was no stratification of salinity. During the SEM season, the vertical salinity distribution near the bottom of the water demonstrated stratification. During the NWM season, the salinity of the water entering the Java Sea from the South China Sea via the Karimata Strait was lower than that during the SEM season. This high salinity (>32 psu) results from the upwelling in the southern Makassar Strait (Atmadipoera *et al.*, 2020; Purba and Khan, 2019; Utama *et al.*, 2017). In both seasons, mixing freshwater masses from rivers in southern Kalimantan (3°S) lowered the salinity (~ 30.5 psu) of the northern seas. However, this impact was greater during the NWM season. The NWM period was characterized by abundant precipitation. Although the SEM period is distinguished by low precipitation (Yulihastin *et al.*, 2021), the vertical distribution of salinity is more homogeneous.

The CROCO18-SSS models were colder and saltier than the GLORYS12V1 reanalysis and satellite data in both seasons both spatially and vertically. These differences were caused by external forcing (bathymetry, atmosphere, tides, river discharge, and oceanic boundary conditions) and the configuration of each model. Thus, each grid model interacts differently. The horizontal and vertical resolutions of the two datasets also caused model grid interactions that increased the difference between their parameters.

The annual cycles of sea surface temperature (Figure 10a.) and salinity (Figure 10b.) derived from the CROCO18-SSS model were relatively consistent with those of the GLORYS12V1 reanalysis and satellite data, indicating that the CROCO18-SSS model can capture seasonal fluctuations in the Karimata Strait (A1), Java Sea (A2), and Makassar Strait (A3). Figure 10a shows that the sea surface temperatures in the Karimata, Java, and Makassar Straits had two peaks in April and September. Seasonal variations in the sea surface salinity (Figure 10b.) in the Java Sea and Makassar Strait peaked in September. This differs from the Karimata Strait, which peaks during April and October. The seasonal cycles of temperature and salinity in the Karimata, Java, and Makassar Straits are related to seasonal water mass movement from adjacent seas (Kok *et al.*, 2021), such as the South China Sea and Flores Sea.

During the NWM and SEM, cold water masses from the southern South China Sea (SSCS) and Flores Sea influenced the seasonal temperature cycle in the Karimata Strait and Java Sea. The SSCS began advecting cold water in December. Colder water was returned to the Java Sea. This cold-water mass meets the warmer Makassar strait water. This movement ended in March, causing the Karimata Strait and Java Sea temperatures to drop, while the Makassar Strait temperatures rose. In addition to the SSCS, the Flores Sea and Makassar Strait currents cool the Karimata Strait and Java Sea. Currents from the Flores Sea enter the Java Sea in May, bringing cold water masses that remain until October. The direction of the Flores Sea current changed in November, increasing the temperature. During SEM, saltwater masses from the Flores Sea and Makassar Strait influenced the seasonal salinity cycle in the Karimata and Java Seas. This movement made June to October salty. River outflow leads to low salinity along the coast, especially in the vicinity of the river mouths. Throughout the season, the salinity was low. This seasonal cycle of sea surface temperature and salinity describes the southern Sunda Shelf water mass.

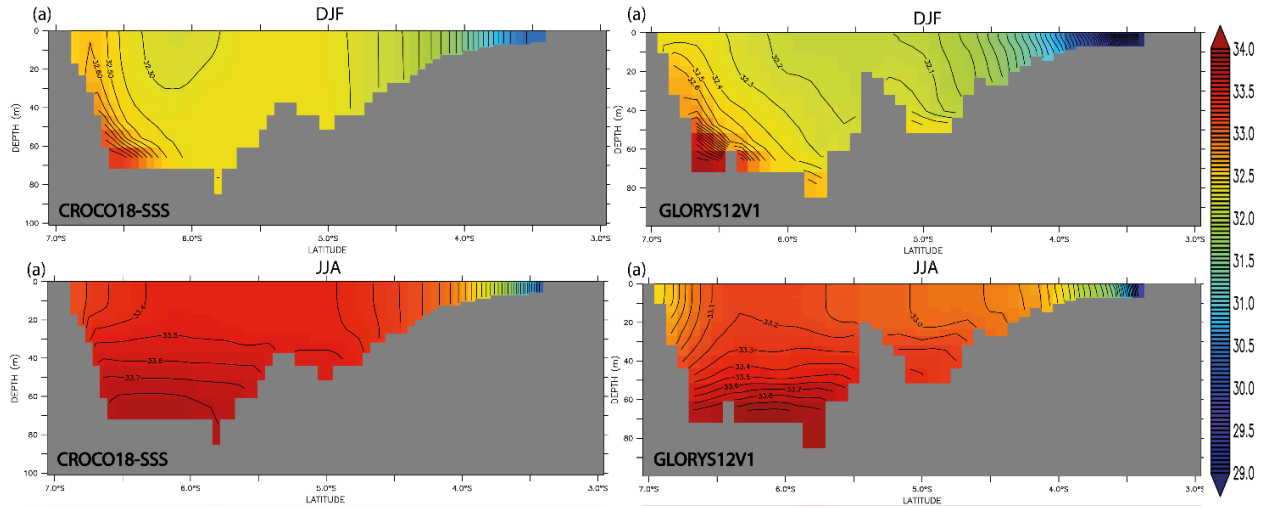

Figure 9. Seasonal vertical distribution of salinity (psu) during the Northwest monsoon (a, b) and (Southeast Monsoon (c, d) derived from CROCO18-SSS (left panel) and GLORYS12V1 (right panel). (Line JJ' in Figure 1.).

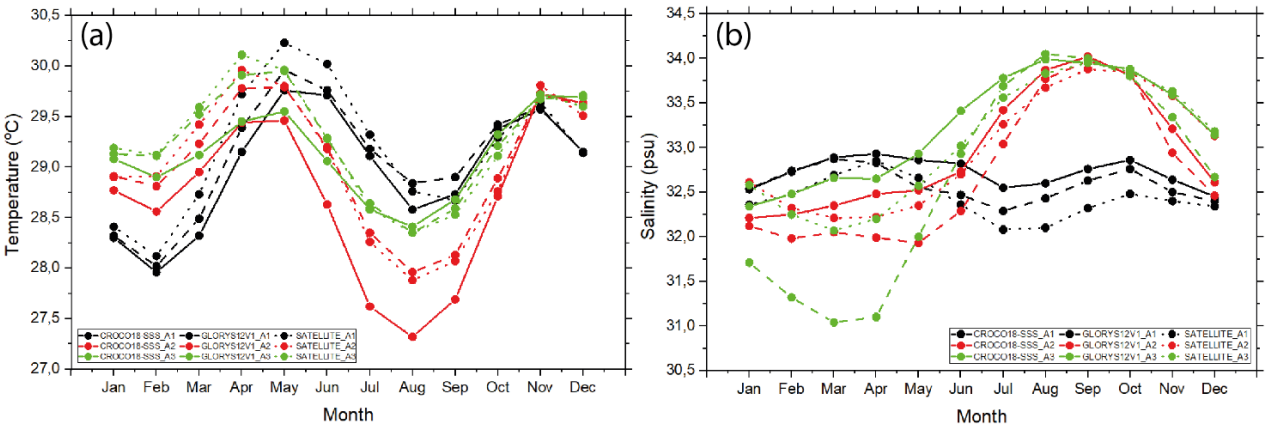

Figure 10. Annual cycle of Temperature (a, ºC) and Salinity (b, psu) derived CROCO18-SSS (solid lines), GLORYS12V1 (dashed lines), and satellite (dot lines) for Region A1 (black), A2 (red), and A3 (green)

Volume Transport

This section evaluates water transport through the KST and MST. Water masses follow both paths from the Pacific to the Indian Ocean (Gordon, 2005; Du and Qu, 2010; Gordon *et al.*, 2012; He *et al.*, 2015; Apriansyah and Atmadipoera, 2020). Figure 11 compares the CROCO18-SSS and GLORYS12V1 reanalysis data for the volume transport of the Karimata (KST) and Makassar straits (MKT). The correlation between KST and MKT volume transport was above 0.9. The RMSD values of KST and MKT were 0.1982 and 0.923, respectively. Evaluation of volume transport in the two transects showed that the CROCO18-SSS model output was significant for the GLORYS12V1 reanalysis product.

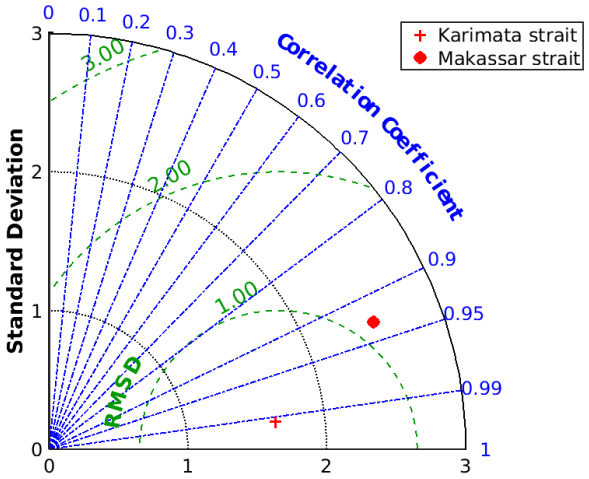

Figure 11. Taylor diagram for volume transport through Karimata strait (KST) and Makassar strait (MKT) derived from CROCO18-SSS and GLORYS12V1 (referred line transect KK' and MM' in Figure 1)

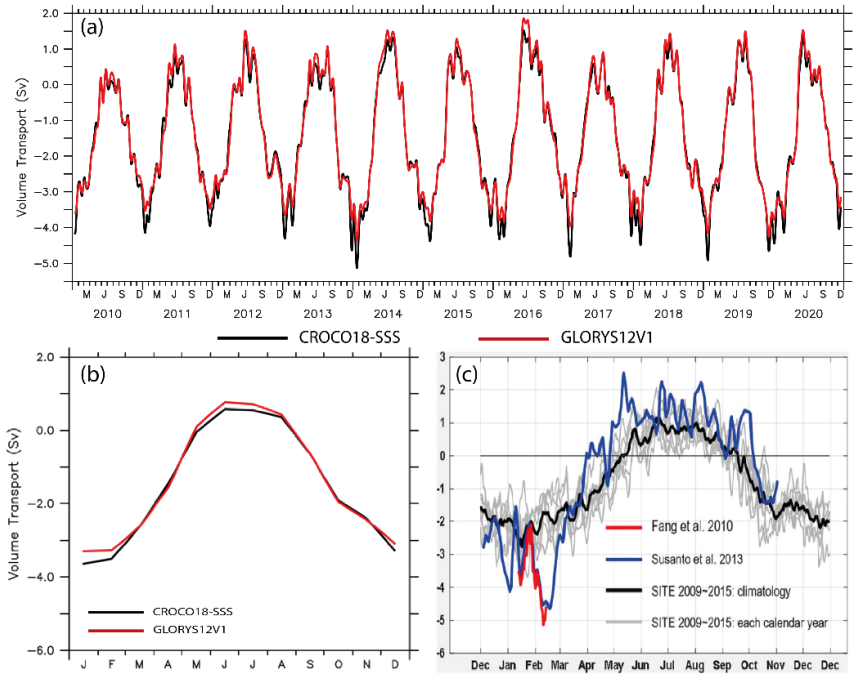

Figure 12. Time series (a) and seasonal variation of volume transport (b) in Karimata Strait with CROCO18-SSS (black line) and GLORYS12V1 (red line). (c) Total volume transport through Karimata Strait, an estimated by Fang *et al.*, (2010) (red line), by Susanto *et al.*, (2013) (blue line); and by Xu *et al.*, (2021) (gray and black lines represent each calendar year and the climatology, respectively). Positive (negative) numbers suggest northerly (southerly) movement through the Karimata Strait.

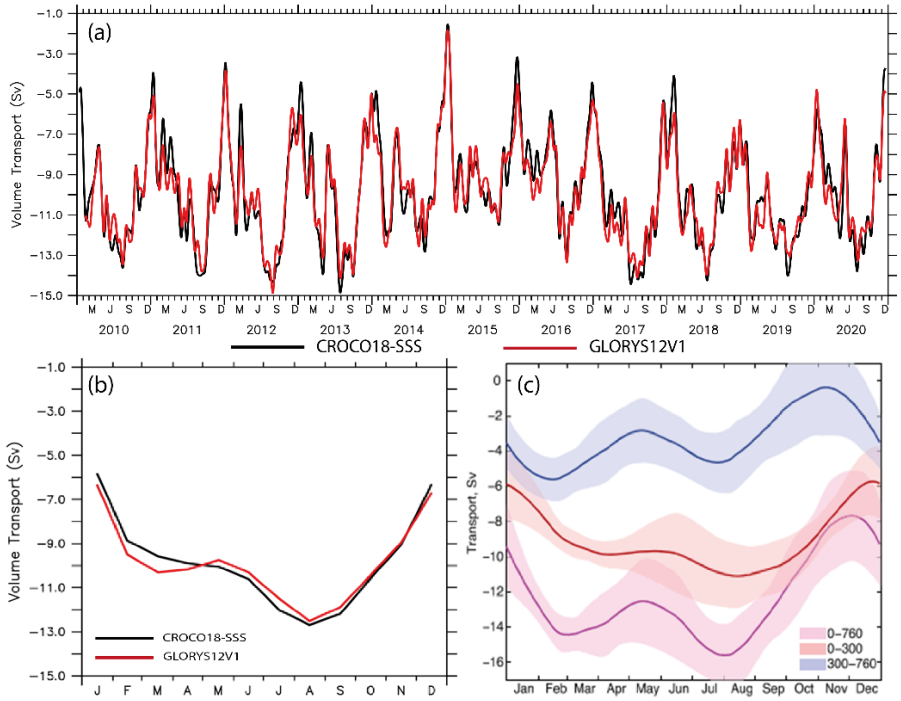

Figure 13. Time series (a) and seasonal variation of volume transport (b) in Makassar Strait with CROCO18-SSS (black line) and GLORYS12V1 (red line). (c) The volume transport through Makassar strait in the indicated levels by (Gordon *et al.*, 2019). The colored envelopes indicate one standard deviation. Negative numbers indicate southward Makassar Strait transport.

Table 2. Previous and current estimation of annual transport (VT; unit = Sv)

Transect	Annual transport (Sv)	Model/Observation	Time period	References
KST	-1.51 ± 1.75	CROCO18-SSS	2010 – 2020	Present study
	-1.43 ± 1.77	GLORYS12V1	2010 – 2020	Present study
	-0.78 ± 0.12	Observation	2009 – 2016	(Xu *et al.*, 2021)
	-0.96	ROMS	2001 – 2015	(Kok *et al.*, 2021)
	-0.48 ± 0.40	INDESO	2008 – 2014	(Apriansyah and Atmadipoera, 2020)
	-0.7	POM	2004 – 2012	(Wei *et al.*, 2016)
	-1.4	BRAN	2004 – 2006	(He *et al.*, 2015)
	-0.58	HYCOM	2003 - 2010	(Gordon *et al.*, 2012)
MKT	-9.81 ± 2.76	CROCO18-SSS	2010 – 2020	Present study
	-9.83 ± 2.41	GLORYS12V1	2010 – 2020	Present study
	-9 ± 0.9	NEMO	1981 – 2012	(Katavouta *et al.*, 2022)
	-10.05	INDESO	2008 – 2012	(Priyono *et al.*, 2020)
	-12.5	Observation	2006 - 2017	(Gordon *et al.*, 2019)
	-12	POM	2004 – 2012	(Wei *et al.*, 2016)

Note: The interannual variation of the model and observation is shown as ± one standard deviation

The calculation of the transport of the two straits reveals the water mass exchange in Karimata (Figure 12.) and Makassar Strait (Figure 13.). Figure 12 shows a comparison of the volume transport in the Karimata Strait. CROCO18-SSS and GLORYS12V1 have almost identical phases and magnitudes. Transport to the south was the highest during the NWM season (December–February). Minimum northward transport occurred during the SEM season (June–August). This is consistent with a previous study (Xu *et al.*, 2021), which stated that water mass movement through the Karimata Strait strengthens southerly during the NWM season and reverses direction towards the north during the SEM period, with annual mean 0.78±0.12 Sv (Figure 12c.).

Figure 13 compares the volume of transport in the Makassar Strait. The CROCO18-SSS and GLORYS12V1 datasets have almost the same phases and magnitudes. Transport to the south was highest

during the SEM season (June–September). The minimum southward transport occurred during the NWM season (December–February). According to Gordon *et al.* (2019), as shown in Figure 13c, the southerly transport achieves its maximum condition (0–760 m) during the SEM season, with an average transport of 12.5 Sv.

Table 2 shows the annual volume transport through the Karimata (KST) and Makassar (MKT) straits based on CROCO18-SSS and previous studies. On an annual scale, estimates of transport through the Karimata and Makassar Straits are -1.51±1.75 Sv and -9.81±2.76 Sv. A comparison of the study's annual transport with that of previous studies indicated a great variation. The estimated annual volume transports from all previous studies in Table 1 are 0.08 – 3.2 Sv and 7.39 – 12.21 Sv for KST and MKT. The current study and GLORYS12V1 reanalysis provided a higher estimate for KST and a lower estimate for MKT. This could be due to the differences in external forcings and configurations from the other data models.

Conclusions

The CROCO model successfully simulated the 3-dimesional ocean circulation model on the southern Sunda Shelf, covering the Java Sea, southern Natuna Sea, Makassar Strait, and Flores Sea, with a horizontal resolution of 1/18^{o} and 40 vertical layers. The CROCO18-SSS results correctly reproduced regional ocean circulation in this region. A comparison of the reanalysis product and satellite-derived (SLA, temperature, salinity, and volume transport datasets) showed a good agreement. The simulated sea level anomaly was similar to those of the satellite and reanalysis datasets. The vertical structure of the zonal current component is comparable to that of other data references. In addition, the seasonal evolution of temperature and salinity with warmer and fresher seawater (colder and saltier) during the northwest monsoon (the southeast monsoon) was also reproduced well by the model. The mean volume transport through the Karimata and Makassar straits has a similar phase and magnitude, and the annual mean volume transport is estimated of about -1.51±1.75) Sv and -9.81±2.76) S and are also comparable to that reported in previous studies.

Acknowledgement

The authors wish to thank the publicly available datasets used in this study, such as the GEBCO, ERA5 ECMWF, GloFas ECMWF, TPXO, GLORYS12V1 reanalysis data, and satellite data. Data were obtained by following the link provided in the manuscript. CROCO and CROCO_TOOLS were obtained from https://www.croco-ocean.org. The author(s) wish to acknowledge the use of the Ferret program for analysis and graphics in this paper. Ferret is a product of NOAA's Pacific Marine Environmental Laboratory. (Information available at http://ferret.pmel.noaa.gov/Ferret/). This research was financed by the Ministry of Education, Culture, Research, and Technology Directorate General of Higher Education for a doctoral dissertation research grant 2022 (contract no. 3645/IT3.L1/PT.01.03/P/B/2022). We also thank the editor and anonymous reviewers for their careful reading of the manuscript and their constructive remarks, which contributed to its improvement.

References

Apriansyah, & Atmadipoera, A.S. 2020. Seasonal Variation of the Sunda Shelf Throughflow, *IOP Conf. Ser.: Earth Environ. Sci.*, 429(1): 012019. https:/doi.org/10.1088/1755-1315/429/1/012019.

Apriansyah, Atmadipoera, A.S., Jaya, I., Nugroho, D. & Akhir, M.F. 2022. Seasonal Oceanographic Changes and Their Implications for the Abundance of Small Pelagic Fishes in the Southern South China Sea, *Reg. Stud. Mar. Sci.*, 54: 102499. https:/doi.org/10. 1016/j.rsma.2022.102499.

Atmadipoera, A.S. & Widyastuti, P. 2015. A Numerical Modeling Study on Upwelling Mechanism in Southern Makassar Strait, *J. Ilmu Teknol. Kelautan Tropis*, 6(2): 355–372. https:/doi.org/10.29244/jitkt.v6i2.9012.

Atmadipoera, A.S., Jasmine, A.S., Purba, M. & Kuswardani, A.R.T.D. 2020. Upwelling Characteristics In The Southern Java Waters During Strong La Nina 2010 And Super El Nino 2015, *J. Ilmu Teknol. Kelautan Tropis*, 12(1): 257–276. https:/doi.org/10.29244/jitkt.v12i1.28977.

Atmadipoera, A.S., Molcard, R., Madec, G., Wijffels, S., Sprintall, J., Koch-Larrouy, A., Jaya, I. & Supangat, A. 2009. Characteristics and Variability of the Indonesian Throughflow Water at the Outflow Straits, *Deep Sea Res. Part I Oceanogr. Res. Pap.*, 56(11): 1942–1954. https:/doi.org/10.1016/j.dsr.20 09.06.004.

Blaas, M., Dong, C., Marchesiello, P., McWilliams, J.C. & Stolzenbach, K.D. 2007. Sediment-Transport Modeling on Southern Californian Shelves: A ROMS Case Study, *Cont. Shelf Res.,* 27(6): 832–853. https:/doi.org/10.1016/j.csr.2006.12.0 03.

de Mello, C., Barreiro, M., Ortega, L., Trinchin, R. & Manta, G. 2022. Coastal Upwelling along the Uruguayan Coast: Structure, Variability and Drivers, *J. Mar. Sys.*, 230: p.103735. https:/doi.org/10.1016/j.jmarsys.2022.1037 35.

Debreu, L., Marchesiello, P., Penven, P. & Cambon, G. 2012. Two-Way Nesting in Split-Explicit Ocean Models: Algorithms, Implementation and Validation, *Ocean Modelling*: 1–21. https:/doi.org/10.1016/j.ocemod.2012.03.003.

Drévillon, M., Lellouche, J-M., Régnier, C., Garric, G., Bricaud, C., Hernandez, O. & Bourdallé-Badie, R. 2021. Quality Information Document For Global Ocean Reanalysis Products GLOBAL_REANALYSIS_PHY_001_030:. 1–52.

Droghei, R., Buongiorno Nardelli, B. & Santoleri, R. 2016. Combining in Situ and Satellite Observations to Retrieve Salinity and Density at the Ocean Surface, *J. Atmos. Ocean. Technol.*, 33(6): 1211–1223. https:/doi.org/10.1175/JTECH-D-15-0194.1.

Du, Y. & Qu, T. 2010. Three Inflow Pathways of the Indonesian Throughflow as Seen from the Simple Ocean Data Assimilation, *Dyn. Atmos. Oceans.,* 50(2): 233–256. https:/doi.org/10.1016/j.dynatmoce.2010.04.001.

Egbert, G.D. & Erofeeva, S.Y. 2002. Efficient Inverse Modeling of Barotropic Ocean Tides, *J. Atmos. Ocean. Technol.*, 19(2): 183–204. https:/doi.org/10.1175/1520-0426 (2002)019<0183:EIMOBO>2.0.CO;2.

Fang, G., Susanto, R.D., Wirasantosa, S., Qiao, F., Supangat, A., Fan, B., Wei, Z., Sulistiyo, B. & Li, S. 2010. Volume, Heat, and Freshwater Transports from the South China Sea to Indonesian Seas in the Boreal Winter of 2007-2008, *J. Geophys. Res. Oceans*, 115(12). https:/doi.org/10.1029/201 0JC006225.

Ganju, N.K. & Sherwood, C.R. 2010. Effect of Roughness Formulation on the Performance of a Coupled Wave, Hydrodynamic, and Sediment Transport Model, *Ocean Modelling*, 33(3-4): 299–313. https:/doi.org/10.1016/j.ocemod.2010.03.003.

Good, S., Fieldler, E., Mao, C., Martin, M.J., Maycock, A., Reid, R., Roberts-Jones, J., Searle, T., Waters, J., While, J. & Worsfold, M. 2020. The Current Configuration of the OSTIA System for Operational Production of Foundation Sea Surface Temperature and Ice Concentration Analyses, *Rem. Sens.,* 12(4): p.720 https:/doi.org/10.3390/rs12040720.

Gordon, A.L. 2005. Oceanography of the Indonesian Seas and Their Throughflow, *Oceanography*, 18(4): 15–27. https:/doi.org/10.5670/oceanog.2005.01.

Gordon, A.L., Huber, B.A., Metzger, E.J., Susanto, R.D., Hurlburt, H.E. & Adi, TR. 2012. South China Sea Throughflow Impact on the Indonesian Throughflow, *Geophys. Res. Lett.*, 39(11): 11602. https:/doi.org/10.1029/2012GL052021.

Gordon, A.L., Napitu, A., Huber, .BA., Gruenburg, L.K., Pujiana, K., Agustiadi, T., Kuswardani, A., Mbay, N & Setiawan, A. 2019. Makassar Strait Throughflow Seasonal and Interannual Variability: An Overview, J. Geophys. Res. Oceans, 124(6): 3724–3736. https:/doi.org/10.1029/2018JC014502.

Gutknecht, E., Dadou, I., Marchesiello, P., Cambon, G., Le Vu, B., Sudre, J., Garcon, V., Machu, E., Rixen, T., Kock, A., Flohr, A., Paulmier, A. & Lavik G. 2013. Nitrogen Transfers off Walvis Bay: A 3-D Coupled Physical/biogeochemical Modeling Approach in the Namibian Upwelling System, *Biogeosciences*, 10(6): 4117–4135. https:/doi.org/10.5194/bg-10-4117-2013.

Hamzah, F., Agustiadi, T., Susanto, R.D., Wei, Z., Guo, L., Cao, Z. & Dai, M. 2020. Dynamics of the Carbonate System in the Western Indonesian Seas During the Southeast Monsoon, *J. Geophys. Res. Oceans,* 125(1): e2018JC014912. https:/doi.org/10.102 9/201 8JC014912.

Harrigan, S., Zsoter, E., Alfieri, L., Prudhomme, C., Salamon, P., Wetterhall, F., Barnard, C., Cloke, H. & Pappenberger, F. 2020. GloFAS-ERA5 Operational Global River Discharge Reanalysis 1979-Present, *Earth Syst. Sci. Data,* 12(3): 2043–2060. https:/doi.org/10.5194/es sd-12-2043-2020.

He, Z., Feng, M., Wang, D. & Slawinski, D. 2015. Contribution of the Karimata Strait Transport to the Indonesian Throughflow as Seen from a Data Assimilation Model, *Cont. Shelf Res.,* 92: 16–22. https:/doi.org/10.1016/j.csr.2014.10.0 07.

Hersbach, H. Bell, B., Berrisford, P., Hirahara, S., Horanyi, A., Munoz-Sabater, J., Nicolas, J., Peubey, C., Radu, R., Schepers, D., Simmons, A., Soci, C., Abdalla, S., Abellan, X., Balsamo, G., Bechtold, P., Biavati, G., Bidlot, J., Bonavita, M., De Chiara, G., Dahlgren, P., Dee, D., Diamantakis, M., Dragani, R., Flemming, J., Forbes, R., Fuentes, M., Geer, A., Haimberger, R., Healy, S., Hogan, R.J., Holm, E., Janiskova, M., Keeley, S., Laloyaux, R., Lopez, P., Lupu, C.,

Radnoti, G., de Rosnay, P., Rozum, I., Vamborg, F., Villaume, S. & Thepaut, J.N. 2020. The ERA5 Global Reanalysis, *Q.J.R. Meteorol. Soc.,* 1 46(730): 1999–2049. https:/doi.org/10.100 2/qj.3803.

Horhoruw, S.M., Fadli, M., Atmadipoera, A.S., Lekalette, J., Nugroho, D.Y., Tatipatta, W.M. & Kainama, F. 2020. Horizontal Structure of Banda Eddies and the Relationship to Chlorophyll-a during South East Monsoon in Normal and ENSO Period on 2008-2010, *IOP Conf. Ser.: Earth Environ. Sci.* 618(1): p.012011. https:/doi.org/10.1088/1755-13 15/618/1/012011.

Ismail, A.M.F. & Ribbe, J. 2019. On the Cross-Shelf Exchange Driven by Frontal Eddies along a Western Boundary Current during Austral Winter 2007, *Estuar. Coast. Shelf Sci.*, 227: p.106314 https:/doi.org/10.1016/j.ecss.20 19.106314.

Katavouta, A., Polton, J.A., Harle, J.D. & Holt, J.T. 2022. Effect of Tides on the Indonesian Seas Circulation and Their Role on the Volume, Heat and Salt Transports of the Indonesian Throughflow, *J. Geophys. Res. Oceans*, 127(8): 1–29. https:/doi.org/10.1029/2022jc018524.

Kok, P.H., Akhir, M.F.M., Tangang, F. & Husain, M.L. 2017. Spatiotemporal Trends in the Southwest Monsoon Wind-Driven Upwelling in the Southwestern Part of the South China Sea, *PLoS ONE*, 12(2): p.e0171979. https:/doi.org/10. 1371/journal.pone.01719 79.

Kok, P.H., Wijeratne, S., Akhir, M.F., Pattiaratchi, C., Roseli, N.H. & Ali, F.S.M. 2021. Interconnection between the Southern South China Sea and the Java Sea through the Karimata Strait, *J. Mar. Sci. Eng.*, 9(10): p.1040 https:/doi.org/ 10.3390/ jmse9101040.

Koropitan, A.F. & Ikeda, M. 2008. Three-Dimensional Modeling of Tidal Circulation and Mixing over the Java Sea, *J. Oceanogr.*, 64(1): 61–80. https:/doi.org/10.1007/s10872-008-000 5-5.

Lellouche, J-M., Le Galloude, O., Greiner, E., Garric, G., Regnier, C., Drevillon, M., Bourdalle-Badie, R., Bricaud, C., Drillet, Y. & Le Traon, P-Y. 2018. The Copernicus Marine Environment Monitoring Service Global Ocean 1/12 • Physical Reanalysis GLORYS12V1: Description and Quality Assessment, *Geophys. Res. Abs.*, 20:p.19806.

Malauene, B.S., Moloney, C.L., Lett, C., Roberts, M.J., Marsac, F. & Penven, P. 2018. Impact of Offshore Eddies on Shelf Circulation and River Plumes of the Sofala Bank, Mozambique Channel, *J. Mar. Sys.*, 185: 1–12. https:/doi. org/10.1016/j.jmarsys.2018.05.001

Nugroho, D., Koch-Larrouy, A., Gaspar, P., Lyard, F., Reffray, G. & Tranchant, B. 2018. Modelling Explicit Tides in the Indonesian Seas: An Important Process for Surface Sea Water Properties, *Mar. Poll. Bull.*, 131: 7–18. https:/doi.org/10.1016/j.marpolbul.2017.06.033.

Nugroho, D., Pranowo, W.S., Gusmawati, N.F., Nazal, Z.B., Rozali, R.H.B. & Fuad, M.A.Z. 2021. The Application of Coupled 3d Hydrodynamic and Oil Transport Model to Oil Spill Incident in Karawang Offshore, Indonesia, *IOP Conf. Ser.: Earth Environ. Sci.,* 925(1): p.012048. https:/doi.org/ 10.1088/1755-1315/925/1/0 12048.

Nuryanto, D.E., Pawitan, H., Hidayat, R. & Aldrian, E. 2016. Heavy Rainfall Distributions Over Java Sea in Wet Season, *Procedia Environ. Sci.*, 33: 178–186. https:/doi.org/10.1016/j.proenv.20 16.03.068.

Penven, P., Marchesiello, P., Debreu, L. & Lefèvre, J. 2008. Software Tools for Pre- and Post-Processing of Oceanic Regional Simulations, *Environmental Modelling and Software*, 23(5): 660–662. https:/doi.org/10.1016/j.envsoft. 20 07.07.004.

Purba, N.P. & Khan, A.M.A. 2019. Upwelling Session in Indonesia Waters, *World News Nat. Sci.*, 25: 72–83.

Ramadhan, H., Nugroho, D., Nurjaya, I.W. & Atmadipoera, A.S. 2021. Influence of River Discharge on Circulation and Tidal Process in the Java Sea, Indonesia, *IOP Conf. Ser.: Earth Environ. Sci.,* 944(1): p.012068. https:/doi.org /10.1088/1755-1315/944/1/ 012068.

Sarr, A.C., Sepulchre, P. & Husson, L. 2019. Impact of the Sunda Shelf on the Climate of the Maritime Continent. *J. Geophys. Res. Atmos.* 124: 2574-2588. https://doi.org/10.1029/20 18JD02997

Shchepetkin, A.F. & McWilliams, J.C. 2005. The Regional Oceanic Modeling System (ROMS): A Split-Explicit, Free-Surface, Topography-Following-Coordinate Oceanic Model, *Ocean Model.,* 9(4): 347–404. https:/doi.org/10.10 16/j.ocemod.2004.08.002.

Susanto, R.D., Ffield, A., Gordon, A.L. & Adi, T.R. 2012. Variability of Indonesian Throughflow within Makassar Strait, 2004-2009, *J. Geophys.*

Res. Oceans, 117(9): C09013. https:/doi.org/10.1029/2012JC008096.

Susanto, R.D., Wei, Z., Adi, R.T., Fan, B., Li, S. & Fang, G. 2013. Observations of the Karimata Strait Througflow from December 2007 to November 2008, *Acta Oceanologica Sinica*, 32(5): 1–6. https:/doi.org/10.1007/s13131-013-0307-3.

Taburet, G., Sanchez-Roman, A., Ballarotta, M., Pujol, M.I., Legeais, J.F., Fournier, F., Faugere, Y. & Dibarboure, G. 2019. DUACS DT2018: 25 Years of Reprocessed Sea Level Altimetry Products, *Ocean Sci.*, 15(5): 1207–1224. https:/doi.org/10.5194/os-15-1207-2019.

Taylor, K.E. 2001. Summarizing Multiple Aspects of Model Performance in a Single Diagram, *J. Geophys. Res. Atmos.,* 106(D7): 7183–7192. https:/doi.org/10.1029/2000JD900719.

Thomson, R.E. & Emery, W.J. 2014. Data Analysis Methods in Physical Oceanography. Third Edition. https:/doi.org/10.1016/C2010-0-663 62-0.

Tozuka, T., Qu, T., Masumoto, Y. & Yamagata, T. 2009. Impacts of the South China Sea Throughflow on Seasonal and Interannual Variations of the Indonesian Throughflow, *Dyn. Atmospheres Oceans*, 47(1-3): 73–85. https:/doi.org/10.1016/j.dynatmoce.2008.09.001.

Tranchant, B., Reffray, G., Greiner, E., Nugroho, D., Koch-Larrouy, A. & Gaspar, P. 2016. Evaluation of an Operational Ocean Model Configuration at 1/12° Spatial Resolution for the Indonesian Seas (NEMO2.3/INDO12) – Part 1: Ocean Physics, *Geosci. Model Dev.,* 9(3): 1037–1064. https:/doi.org/10.5194/gmd-9-1037-20 16.

Uchiyama, Y., McWilliams, J.C. & Shchepetkin, A.F. 2010. Wave-Current Interaction in an Oceanic Circulation Model with a Vortex-Force Formalism: Application to the Surf Zone, *Ocean Model.*, 34(1-2): 16–35. https:/doi.org/10.1016/j.ocemod.2010.04.002.

Utama, F.G., Atmadipoera, A.S., Purba, M., Sudjono, E.H. and Zuraida, R. 2017. Analysis of Upwelling Event in Southern Makassar Strait, *IOP Conf. Ser.: Earth Environ. Sci.,* 54(1): p.012085 https:/doi.org/10.1088/1755-1315/54/1/012085.

Weatherall, P., Marks, K., Jakobsson, M., Schmitt, T., Tani, S., Arndt, J.E., Rovere, M., Chayes, D., Ferrini, V. & Wigney, R. 2015. A New Digital Bathymetric Model of the World's Oceans, *Earth Space Sci.*, 2(8): 331–345. https:/doi.org/10.1002/2015EA000107.

Wei, J., Li, M.T., Malanotte-Rizzoli, P., Gordon, A.L. & Wang, D.X. 2016. Opposite Variability of Indonesian Throughflow and South China Sea Throughflow in the Sulawesi Sea, *J. Phys. Oceanogr.,* 46(10): 3165–3180. https:/doi.org/10.1175/JPO-D-16-0132.1.

Wyrtki, K. 1961. Physical Oceanography of the Southeast Asian Waters., Scietific Resultas of Marine Investigations of the South China Sea and the Gulf of Thailand, 2, p. 195.

Xu, T.F., Wei, Z., Susanto, R.D., Li, S.J., Wang, Y.G., Wang, Y., Xu, X.Q., Agustiadi, T., Trenggono, M., Sulistyono, B., Setiawan, A., Kuswardani, A. & Fang, G.H. 2021. Observed Water Exchange Between the South China Sea and Java Sea Through Karimata Strait, *J. Geophys. Res. Oceans,* 126(2): p.e2020JC016608.. https:/doi.org/10.1029/2020JC016608.

Yulihastin, E., Putranto, M.F. & Suaydhi. 2021. The Effect of Local Forcing on Anomalously High Rainfall during Dry Season in Java, Indonesia, *J. Southwest Jiaotong Univ.*, 56(3): 32–42. https:/doi.org/10.35741/issn.0258-2724.56. 3.3.